

Development of a Hypodermic Needle-based Point-of-Care Device for the Detection of Vitamin-B12 and Vitamin-C from Cancer-Induced Sprague Dawley Rat Urine Samples

Rajath Othayoth ¹ , Mahendran Botlagunta ^{1,2,*} 

¹ Department of Biotechnology, K L E F (Koneru Lakshmaiah Education Foundation), Andhra Pradesh, India; rajath.biotech@gmail.com (R.O.);

² School of Biosciences Engineering and Technology, VIT Bhopal University, Bhopal, India; bmnchowdary@gmail.com (M.B.);

* Correspondence: bmnchowdary@gmail.com (M.B.);

Scopus Author ID 24447969400

Received: 17.11.2022; Accepted: 8.01.2023; Published: 19.03.2023

Abstract: Vitamin deficiency is a common side effect of chemotherapy-induced cancer fatigue. The current antibody-based diagnostic kits are only used to measure the status of vitamins in cancer patients with painful procedures. And these tests are expensive and time-consuming. Hence, it is essential to measure the status of vitamins in cancer patients using point-of-care (POC) devices. We designed and developed an affordable, recyclable POC testing device in this study using ANSYS software version 2021 R2. The polyvinylidene fluoride (PVDF) membrane-based piezoresistive cantilever sensor was placed inside a hypodermic needle case. This sensor was coated with ascorbate oxidase (AO), hydrogen peroxide (H₂O₂), and luminol, and the oxidation of micronutrients in the tumor-induced rat's urine sample was measured using a digital multimeter. The maximum amount of deflection was observed when the sensor was loaded with vitamins B12 and C injected rat's urine. The assay exhibited good resistance responses toward target vitamins B12 and C. Moreover, our strategy provided acceptable reproducibility, precision, high specificity, and good accordance with the commercial kit for detecting micronutrients in cancer patients. This device helps detect the vitamins from a cancer patient's urine samples, a non-invasive way of carrying out sensitive diagnostic tests.

Keywords: cancer diagnosis; vitamins; point-of-care (POC) testing; hypodermic needle; digital multimeter.

© 2023 by the authors. This article is an open-access article distributed under the terms and conditions of the Creative Commons Attribution (CC BY) license (<https://creativecommons.org/licenses/by/4.0/>).

1. Introduction

In the last few years, the survival rates of cancer patients have exponentially increased. And these survivors may experience temporary or permanent side effects of chemotherapy or other cancer treatments [1]. It is mainly because cancer patients often consume vitamin and mineral-deficient food. Hence, most of these patients have various nutrient deficiencies [2]. The patient follow-ups by doctors mainly focus on the cancer reoccurrence and not on identifying the nutrition concerns regarding post-cancer treatments. The nutritional assessment is essential for the cancer prognosis, such as response rate and survival [3]. The studies of nutritional screening of patients undergoing adjuvant or neo-adjuvant chemotherapy are very limited to analyzing cancer patients' nutritional status [4]. Nutritional deficiencies are

traditionally checked through blood tests like finger-prick or venous blood tests [5]. Few tests are available using saliva and urine, but they are not effective during cancer therapy [6-8]. It is because patients often suffer when the blood sample is drawn during each time follow-up [9]. Moreover, the diagnosis of samples is possible only in the laboratory, so the need for clinical visits is also high for the patients [10].

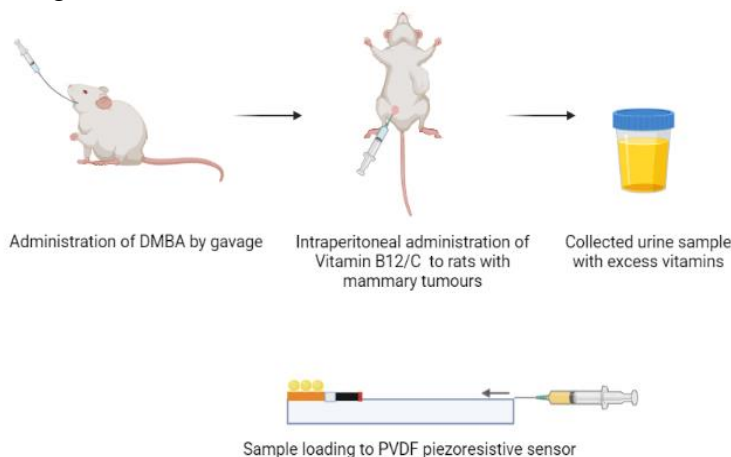
On the other hand, these methods also have many disadvantages long time analysis, sample preparation, large sample volume, expensive and high-end instrumentation, and also require highly trained personnel [11]. A non-invasive way of carrying out the diagnostic test is required in such scenarios. So novel and cost-effective sensors are a valuable alternative option because of their sensitivity, reliability, and reproducibility [12]. Based on the piezoresistive effect, oxidation, and reduction reaction with the analyte, these sensors detect Vitamin B12 and Vitamin C [13, 14].

Recently, many novel sensors have been proposed to detect water-soluble vitamins Vitamin B12 and C [15]. The flexible PVDF-based sensors are inexpensive, simple to fabricate, lightweight, and disposable [16]. The piezoresistive effect is a change in the electrical resistivity of metal when mechanical strain is applied. And the piezoresistive effect causes a change only in electrical resistance, not electric potential [17]. The working principle of the PVDF-based membrane sensor is based on the piezoresistive inducing strain/stress. Based on the piezoresistive effect, the strain/stress can be converted into a resistance change by the sensing component, easily detected by the digital multimeter [18]. To realize a flexible system, a PVDF substrate is used instead. The PVDF cantilever beam is used to let the force applied to it. The graphite is placed on the cantilever beam as the sensing component. When force is applied to the cantilever beam, the stress of the beam will change sensitively [19]. And these sensors can be operated at higher temperatures and are more suitable for harsh environments. The approach combines analysis of PVDF-based piezoresistive sensors with simulation by giving different parameters using the software ANSYS [20, 21].

As per World Health Organization (WHO) suggestions, the ancient and traditional diagnostic techniques offered to develop countries are currently replacing by affordable, user-friendly, fast, point-of-care (POC) techniques [22]. These devices have drawn considerable attention and developed rapidly in recent decades because of their portability and affordability [23]. And every day, new protocols and strategies are developed to improve their specificity and sensitivity [24]. The main key point of these inventions is to detect highly effective and sensitive signals that are generated efficiently in a short period [25]. There are several POC devices have been developed to measure different physical and biological parameters by sensing their pressure, weight, temperature, and color changes [26]. Pressure and weight have been used to measure biological, chemical, or biochemical reactions [27]. The pressure and weight sequentially increased in a sealed hypodermic needle system by generating a very minute quantity of gas through oxidation reactions [28]. There are several gas-generating reactions have already been established in POC testing devices [29]. In that, hydrogen peroxide (H_2O_2) to Oxygen (O_2) is widely used for studies due to its high yield and production of nontoxic gases [30]. The reactions of ascorbate oxidase (AO), hydrogen peroxide (H_2O_2), and luminol produced oxygen, which increases pressure and piezoresistivity in the PVDF sensor [31]. The decomposition of ascorbate oxidase (AO) and hydrogen peroxide (H_2O_2) increases the sensitivity and also shortens the detection time [32]. So the pressure change can easily be detectable in this POC device, and the final signal readout will be simple, sensitive, and effective during diagnosis [33, 34]. The flexible pressure sensors exhibit high sensitivity

compared to the conventional ones [35]. And also they can be easily fabricated by using different substrates according to various shapes and sizes. PVDF is an effective substrate material due to its low cost and flexibility [36]. There have been many studies on paper-based pressure sensors for various healthcare applications [37]. With such a high specificity, sensitivity, and affordability, PVDF-based flexible pressure sensors can improve the efficacy of POC-based diagnosis testing [38].

Point-of-care (POC) diagnosis is an easy and fast method of analysis in health care, food, and environmental field [39]. The POC devices are mainly used to detect the biomarkers associated with various diseases [40]. These devices have various advantages over traditional diagnoses, such as mass spectrometry, fluorescence assay, and electrochemical analysis [41]. And they are very efficient and economical compared to large types of equipment during diagnosis [42]. But still, there are many challenges in POC development, like specificity and sensitivity [43]. The key factors during POC testing are detecting biochemical reactions and biomolecular recognition. Most physical quantities are very easy to measure, but converting reactions and recognition of biological samples into measurable physical quantities requires high-end sensing [44]. The production of gas during the hydrogen peroxide (H_2O_2) to oxygen (O_2) reduction reaction is considered more efficient and environmentally friendly compared to other gas-producing reactions [45]. The conversion of signals is based on the pressure produced by the decomposition of ascorbate oxidase (AO) and hydrogen peroxide (H_2O_2) inside the POC device [46]. And the pressure created in the air is converted to different electro-mechanical signals through the transduction principles like piezoresistivity [47]. Therefore, we propose the strategy of synergistic action of pressure and piezoresistivity. Many devices have been developed based on pressure-based POC testing [48]. But the multifunction response in the single POC device has a great future in sensor development [49, 50]. Therefore, using environmentally friendly and affordable PVDF membrane as a substrate has great scope in developing flexible piezoresistive pressure sensors [51]. The polyvinylidene fluoride (PVDF) membrane is a flexible piezoelectric polymer with wide material properties like high pressure and light sensitivity [52]. And the PVDF membrane surface with graphite is highly conductive to electrical signals during sensitive biochemical reactions [53]. The released oxygen (O_2) creates pressure on the graphite and acts as an external force on the flexible PVDF membrane pressure sensor [54]. The sensor further generates a piezoresistivity on the PVDF membrane, which sequentially increases resistance in the hypodermic needle case. The resistance change is measured using a digital multimeter (DMM).



Scheme 1. Schematic Illustration of Point-of-Care testing with the urine samples of breast cancer-induced S.D. rats injected with Vitamin B12 and Vitamin C.

Thus, the presence and concentration of micronutrients like Vitamin B12 and Vitamin C can be quantitatively detected by monitoring the resistance change that occurred during the biochemical reactions. The ultra-sensitive detection of Vitamin B12 and Vitamin C from breast cancer-induced rat urine samples is used to confirm the efficacy, specificity, and sensitivity of our novel POC device (Scheme 1).

2. Materials and Methods

2.1. Working principle.

The main working principle of the PVDF-based membrane sensor is based on the piezoresistive effect. Traditional force and pressure sensors use a cantilever beam that can induce stress and strain while applying different loads. The stress or strain is converted to the resistance change by piezoresistive effect by sensing element, which different electrical instruments can easily analyze. In consideration of flexibility, affordability, and sensitivity PVDF membrane is used as a substrate instead of other conventional materials. The point load weight followed by pressure applied to the PVDF cantilever beam sequentially increases during the biological sample (Tumour induced rat's urine) loading in each second. Graphite-coated area in the PVDF membrane acted as a sensing component in the device. The stress in the cantilever beam changes sensitively according to the weight and pressure applied.

2.2. Device structure.

The MEMS-based piezoresistive cantilever was designed using ANSYS software version 2021 R2. The structure PVDF membrane-based-sensor is shown in Figure 1. In this structure, a copper strip electrode, silver ink electrode, and graphite electrode are located in the PVDF cantilever beam. The sensing part is coated with graphite. The weight (Sample) is applied to this cantilever beam, and the graphite part will get a mechanical strain or stress; this further induces a change in the resistance. The oxidation reaction of the sample with the ascorbate oxidase (AO), hydrogen peroxide (H_2O_2), and luminol also makes a resistance change. Measuring the resistance change can reflect the magnitude of the samples' applied weights and the oxidation reaction's intensity.

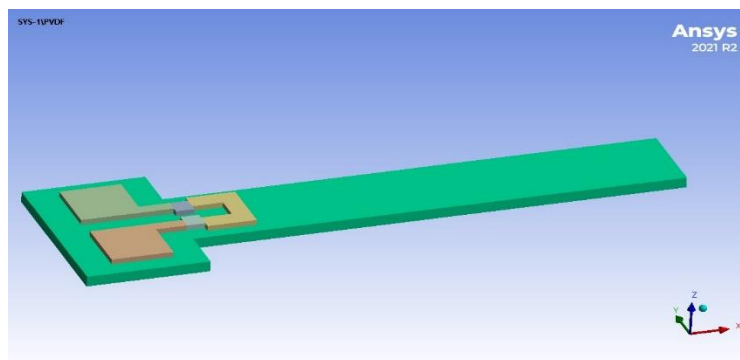


Figure 1. Structure layout of PVDF membrane sensor.

2.3. Fabrication process.

The fabrication process of the PVDF membrane-based flexible piezoresistive sensors is shown in Figure 2.

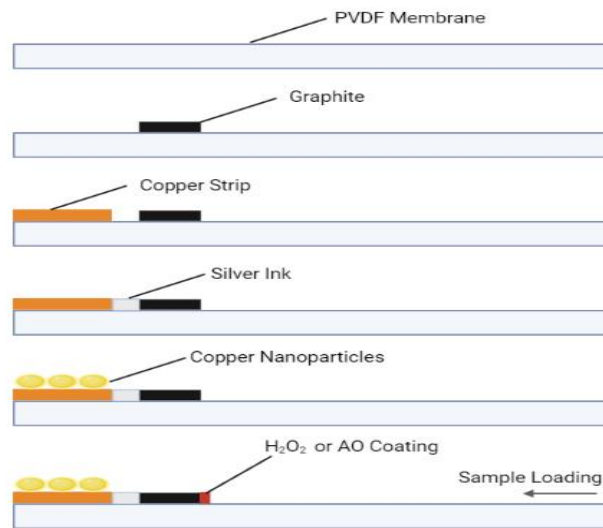


Figure 2. The fabrication process of PVDF membrane-based piezoresistive sensors.

The PVDF membrane (0.8 mm thickness) is used as substrate material and cut into the desired shape using scissors. The PVDF membrane cantilever beam has length, depth, and height of 10mm, 3mm, and 0.8 mm, respectively (Figure 3).

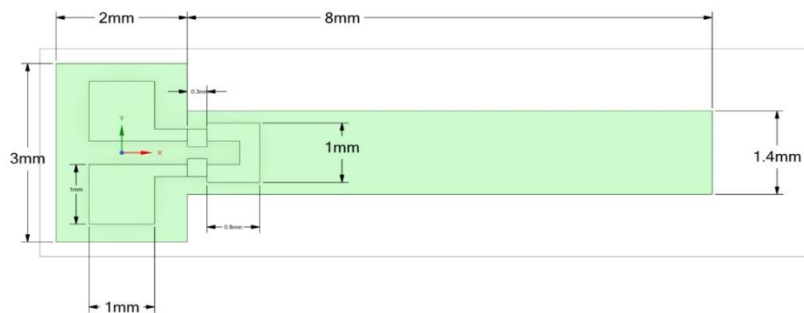


Figure 3. The geometry of the PVDF membrane sensor.

In the ANSYS software version 2021 R2, the dimensions and layers were applied with a thickness of 0.2mm each. The PVDF membrane sensor's geometry is formed by adding different piezoresistive materials to the model (Table 1).

Table 1. Comparison of piezoresistive materials.

Materials	Young's Modulus (GPa)	Poisson's Ratio	Density (kg/m ³)
Copper	117	0.33	8933
Silver	10.5	0.37	10500
Graphite	27.6	0.23	2250
PVDF	1.10	0.35	1780

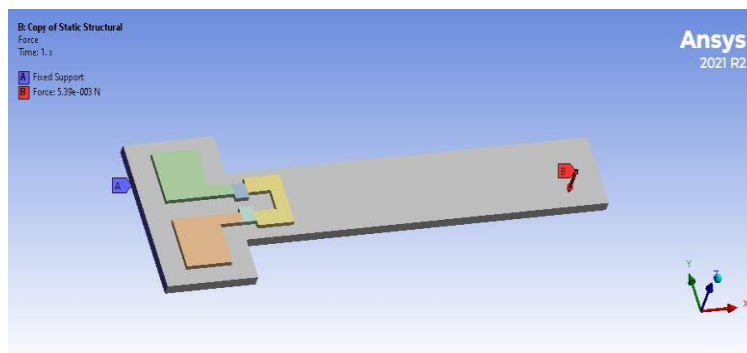


Figure 4. The point loading in the cantilever beam.

The head side of the cantilever beam is placed with Copper, Silver, and Graphite materials. The materials were assigned according to domains in the ANSYS window. To get better output from the design, the cantilever beam is analyzed with given piezoresistive materials by applying weight at the cantilever's tail end (point load) (Figure 4).

The graphite resistors are made by using a 7B pencil and prepared graphite paste. And contact pads are made by using copper nanoparticles (less than 200 nm) coated in low-resistivity copper strips. Silver ink is used as a linkage between graphite resistors and copper pads to enhance its electrical connection. The cantilever deflection and displacement were observed for the applied weights ranging from 30 mg to 550 mg (1 drop of sample to 10 drops of the sample). The beam's free end gets displaced when input weight is applied, and an oxidation reaction happens (Figure 5).

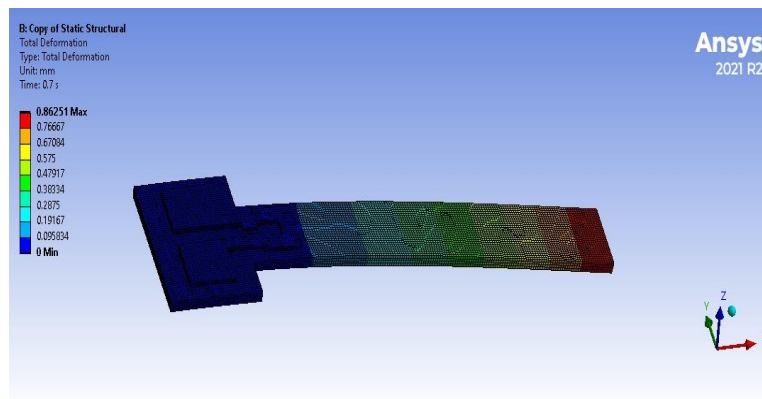


Figure 5. The displacement observed in the cantilever beam.

Three piezoresistive materials are used in work on the PVDF membrane. Different input loads were analyzed for copper, Silver, and Graphite materials. This work is concentrated mainly on the maximum amount of deflection observed for the applied weights and the piezoresistive effect and oxidation reaction that occurred with the loaded urine sample (Figure 6).

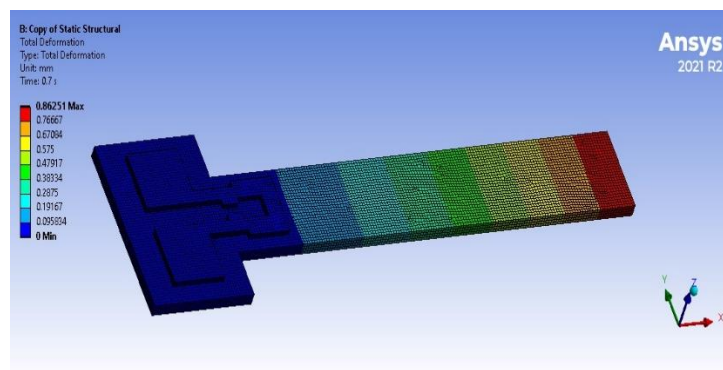


Figure 6. Total deformation.

The resistance change due to deflection is monitored by a digital multimeter (DMM). The PVDF membrane-based sensor was then assembled in a hypodermic needle with a small hole on the side. One end of the copper contact pad through the hole was connected with the digital multimeter to measure the change in resistance. Then the hole was further sealed with ethylene-vinyl acetate (EVA) to conduct the gas very easily during biochemical reactions and prevent the spillage of biological samples.

Vitamin B12 and Vitamin C were detected by this POC device based on a flexible piezoresistive sensor. Before sample loading, the end of the graphite resistor in the PVDF membrane was coated with 20 μl of ascorbate oxidase (AO) (For Vitamin C detection), hydrogen peroxide (H_2O_2) (For Vitamin B12 detection), and luminol, respectively, and incubated at 37°C for 48 hours. Then 0-100 μl of tumor-induced rat urine sample pellet (centrifugation 14000 rpm at 4°C for 25 minutes) after diluting with distilled water loaded to the PVDF membrane through a hypodermic needle, and gas was started to produce after 7 minutes. The resistance change that occurred during the reactions was monitored through DMM continuously.

2.4. Preparation of copper nanoparticles and graphite paste.

The graphite paste was prepared by mixing 10 g of graphite powder (Sigma-Aldrich chemicals Private Ltd., Bangalore, India) with 4 ml of paraffin oil (Sigma-Aldrich chemicals Private Ltd., Bangalore, India) in a mortar with a pestle. The paste was formed after 5 minutes (Figure 7B). Then the formed paste was dried in a glass slide and incubated at 37°C for 48 hours. Dried paste is used for further use. The copper nanoparticles were prepared by dissolving 1 mg of copper nanopowder (Sigma-Aldrich chemicals Private Ltd., Bangalore, India) in 1 ml of ethanol. These copper nanoparticles were used to coat the copper strip (Figure 7C).

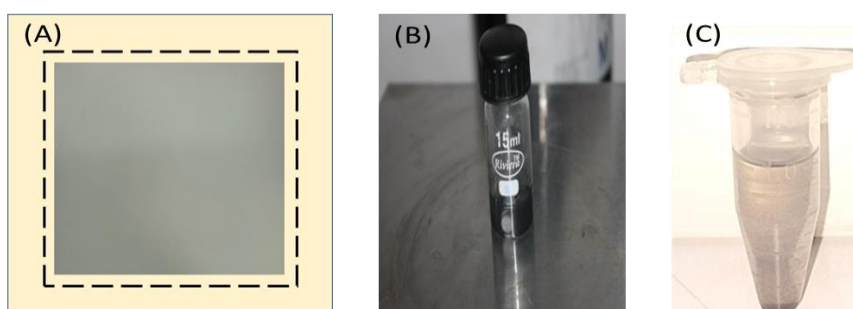


Figure 7. Photographs of (A) PVDF membrane; (B) Graphite paste; (C) Copper nanoparticles.

2.5. Characterization studies.

The diameters of Copper nanoparticles are identified by dynamic light scattering using a Particle size analyzer (Brookhaven Instrument Crop. Model- Zeta Plus 460). The dynamic light scattering is done with a wavelength of 658 nm at 25°C with an angle detection of 90°C . The zeta potential of nanoparticles was determined by using Zeta potential analyzer (Brookhaven Instrument Crop. Model- Zeta Plus 460). The morphology of the PVDF membrane, Copper nanoparticles, and Graphite paste was observed using a scanning electron microscope (Carl Zeiss Model Supra 55, Germany). The PVDF membrane, Copper nanoparticles, and Graphite paste were dried on an aluminum disk at room temperature and then further coated with gold using a Cressington sputter coater. Transmission electron microscopy (TEM), JEOL JEM 2100 PLUS, was used to assess the morphology of the copper nanoparticles. TEM analysis was carried out by placing a drop containing a suspension of nanoparticles onto a copper network covered by carbon and enabling water dissipation in a vacuum-enabled dryer. The grid with nanoparticles was scanned to obtain the images. Fourier transform infrared (FT-IR) spectra were analyzed using a spectrometer (PerkinElmer) at 4000–400 cm^{-1} resolution. The tumor-induced rat urine samples were taken before and after the Vitamin B12 and Vitamin C injection and mixed with potassium bromide to analyze the

vitamins and cisplatin present in the urine. The thermal behavior of the PVDF membrane, Copper nanoparticles, and Graphite paste was analyzed by differential scanning calorimetry (DSC 4000, Perkin Elmer). Approximately 4-8mg of samples were weighed and scanned in a temp range of 0-400⁰C with a heating rate of 10⁰C/min per cycle. The inert atmosphere was maintained in ambient air. X-ray diffraction (XRD) pattern of PVDF membrane, Copper nanoparticles, and Graphite paste was recorded using Bruker D8 Focus diffractometer functioning at a voltage of 40 kV and a current of 35 mA with Cu K α radiation ($\lambda = 1.54060$ Å). The XRD patterns were obtained in fixed time mode with a scan duration of 30 minutes and 2 θ ranging from 5⁰ to 9⁰ at room temperature.

2.6. Mechanical properties of the PVDF cantilever beam.

The sample weights (urine) were applied to the end of the PVDF cantilever beam, creating forces at the free end. Then deflections were observed in the beam's free end due to the point loads. As a result, the PVDF membrane stiffness was 0.005 N/mm. The Young's modulus of the PVDF membrane material can also be calculated by using the following equation:

$$E = \frac{4L^3 F}{\delta W H^3} \quad (1)$$

In this equation, E is Young's modulus of the PVDF membrane, F is the force created while applying weights, δ is the deflection of the beam, and L, W, and H are the length, width, and height (thickness) of the PVDF membrane respectively. Young's modulus of the PVDF membrane was 1.103 GPa.

2.7. Electrical properties of graphite resistor.

The prepared graphite resistor current-voltage (I-V) characteristics were measured using the Keithley 2450 source meter under conditions like relative humidity (50%-60%) and ambient temperature at 25 °C.

2.8. Animal studies.

The standard laboratory rodent species, rats, were used as a reliable test model to induce the tumor and assess the response toward vitamins. The Sprague Dawley (S.D) rat's strain, 40 females, 6-8 weeks of age, was chosen for the experiment. The body weights of the rats are measured by using Denver Instrument SI-4001. Initial weights (Before the experiment) of the rats were 195g-201g and maintained on a 12-hr light/12-hr dark cycle. The 7,12-Dimethylbenz[a]anthracene (DMBA), 900mg dissolved in 45 ml of soya oil and administered through intragastric route to all female S.D. rats and observed for tumor induction up to 8 weeks. Tumor induction began at 4-6 weeks and was confirmed by the palpation of mammary tumors. Further, Vitamin B12 and Vitamin C were administered through the intraperitoneal route to the rats by using a graduated syringe with a needle. The experiment was continued for 3 weeks for 3 cycles. In each cycle, urine samples were collected.

2.9. Collection of urine samples.

The tumor-induced rat's urine was collected in a clean, dry 5ml plastic test tube. A gentle rub was applied to collect urine, starting below the rat's ribcage and ending at its pelvic bone when the rats were calm in the human palm. The pressure in the pelvic bone created

pressure on the rat's urinary bladder. This process was continued several times until they urinated. The rat's urethra was kept above the test tube for urine collection at different time intervals. The urine samples were collected daily from each tumor-induced rat during the experiment.

2.10. Chemical analysis of rat urine.

The copper strips were pasted on one side of the glass slides. Then 20 μ l of H₂O₂, AO, luminol, and rat urine sample were sequentially added for 15-minute intervals to the glass slide. The slides were then incubated at 37⁰C for 24 hours.

2.11. Chemiluminescence assay.

Chemiluminescence reactions were performed in a 96-well optiplate placed in a microplate reader. The plate was loaded with 0-100 μ l of tumor-induced rat urine before and after vitamins injections, ascorbate oxidase (AO) and luminol, respectively, for vitamin C detection and ascorbate oxidase (AO), hydrogen peroxide (H₂O₂), and luminol for Vitamin B6 and Vitamin B12 detection. The chemiluminescence was measured with a multimode plate reader (PerkinElmer). And the graphs were plotted using the graph pad prism software (Graph Pad Software Inc., CA, USA).

2.12. Performance of hypodermic needle-based POC device.

The change in resistance of the graphite resistor in the PVDF membrane sensor cantilever beam was measured according to different weights applied on the tail end of the sensor. The applied weights ranged from 30 mg to 550 mg (1 drop of the sample to 10 drops of the sample). And the change in resistance was measured by using a digital multimeter (Fluke, USA).

2.13. Statistical analysis.

All experiments were carried out three times, and the findings are shown as mean \pm standard deviation. We used a one-way analysis of variance to determine the statistical significance of the data, with a significance level of $p < 0.05$.

3. Results and Discussion

3.1. Fabrication process.

To get better output from the design, the cantilever beam is analyzed with given piezoresistive materials by applying weight at the cantilever's tail end (point load). The cantilever deflection and displacement were observed for the applied weights ranging from 30 mg to 550 mg. Resistance was increased by increasing the weights of the sample. The tumor-induced rat urine sample on the PVDF membrane graphite sensor created weight changes and triggered the oxidation process due to ascorbate oxidase (AO), hydrogen peroxide (H₂O₂), and luminol present in the graphite sensor. The piezoresistive effect and biochemical reactions created resistance to change and were monitored through DMM continuously. The pressure also changes inside the hypodermic needle case due to gas production by oxidation reactions. This pressure change is detected by the flexible PVDF membrane pressure sensor and detected by a digital multimeter. The main goal of this work is to develop a user-friendly, portable, and

affordable POC testing device for the ultrasensitive detection of Vitamin B12 and Vitamin C from cancer patients' urine samples. The response to minute changes is crucial to develop a highly sensitive POC device based on pressure sensing and oxidation reactions. The device principle is based on the resistance change and oxidation reaction in the PVDF membrane piezoresistive sensor placed inside a hypodermic needle (Figure 8).

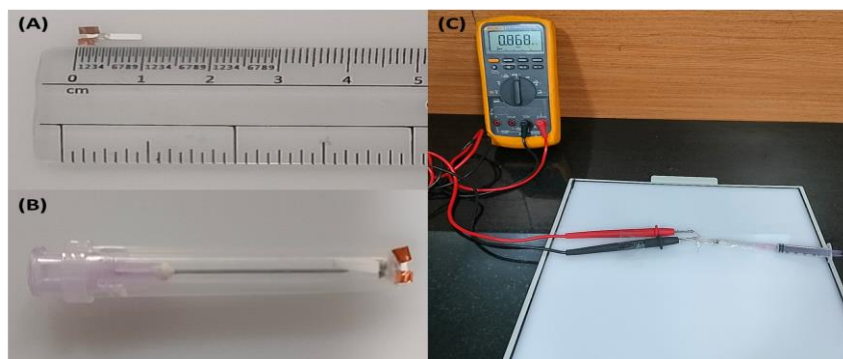


Figure 8. (A) Handmade piezoresistive pressure sensor; (B) Hypodermic needle-based device; (C) POC detection system connected with a digital multimeter.

When a tumor-induced rat urine sample is loaded on the device, a compressive deflection occurs in the area, enhancing the conductive sites. This increases the current at a fixed applied potential. And when the cantilever sensor regains its original shape, the contact area and the current reduce drastically by changing the resistance. In the same way, the cantilever beam supports biochemical reactions also. For example, while increasing the rat's urine concentrations, a compressive deformation occurred in the area. It enhanced the sample to react with the H_2O_2 , AO, and luminol at the tip of the graphite sensor. This expedites the deformation and increases the resistance value. The PVDF membrane supports these changes through its porous property. The unique microstructure of the PVDF membrane was an important feature for the POC device to sensitively monitor the oxidation reaction and pressure due to its change in the contact area.

3.2. Characterization studies.

The particle size diameter and zeta potential of the copper nanoparticles are shown in Table 2.

Table 2. Mean diameter, polydispersity index, and zeta potential of Copper nanoparticles.

S. No.	Nanoparticles	Mean diameter (nm)	Polydispersity index	Zeta potential (mV)
1	Cu Nanoparticles	312±8.3	0.185±0.047	25.56 ±0.22mV

The diameter of the copper nanoparticles was 312 ± 8.3 nm. The zeta potential values were analyzed to determine the nanoparticle stability. The zeta potential value was 25.56 ± 0.22 mV. These copper nanoparticles are coated on the copper strip surface and enhance the electrical signal flow. The SEM images showed the morphology of the PVDF membrane, Copper nanoparticles, and Graphite paste. The surface of the PVDF membrane exhibited a rough microsurface, great intact, lesser pores, and rich fibrous growth (Figure 9A). The copper nanoparticles were spherical and well dispersed, and their size was around 300 nm (Figure 9B). The graphite paste surface was irregularly shaped with different size flakes of graphite (Figure 9C).

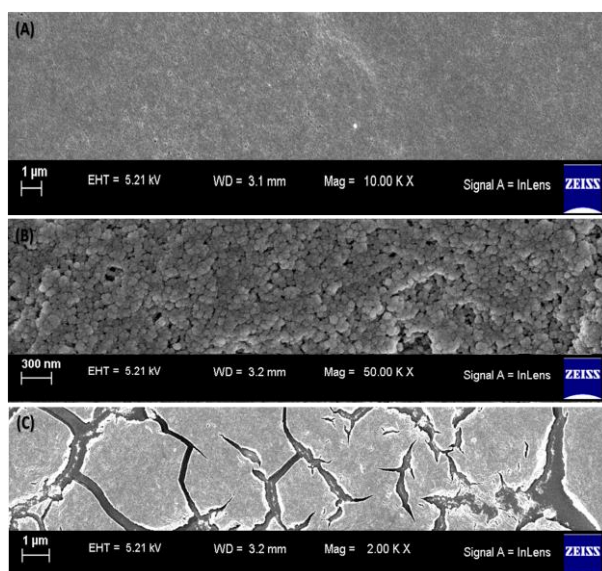


Figure 9. SEM image of (A) PVDF membrane (B) Copper nanoparticles (C) Graphite paste.

The copper nanoparticles were well dispersed and exhibited core structure in the TEM image (Figure 10).

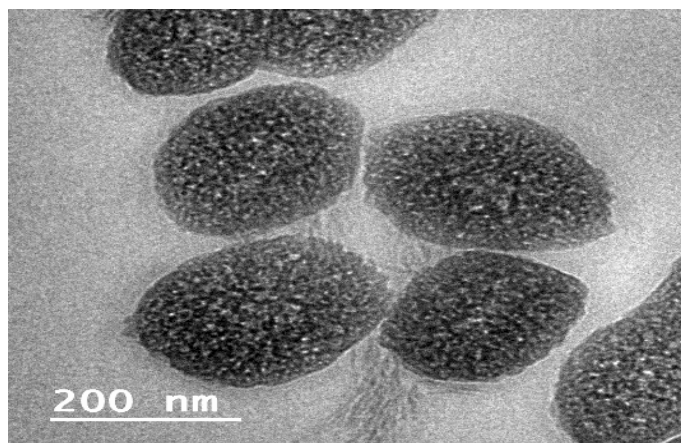


Figure 10. TEM image of Copper nanoparticles.

The SEM and TEM images exhibited the morphology of the PVDF membrane, Copper nanoparticles, and Graphite paste. The PVDF membrane showed lesser pores and rich fibers for easy sample flow through its surface. The copper nanoparticles were spherical in size and well dispersed, and the graphite surface showed irregular-sized flakes. This enhances the electrical characteristics of the graphite sensor.

Fourier transform infrared (FT-IR) spectra of tumor-induced rat urine samples exhibited stretches for control rat urine (Figure 11A). The tumor-induced rat urine covers the 4000–400 cm^{-1} resolution. This spectrum was individually normalized to the urea band at 1639 cm^{-1} resolution. The new peaks, along with the urea peak, were observed at 2983 cm^{-1} and 1394 cm^{-1} for Vitamin B12 injection (Figure 11B). That represents the presence of an excess of vitamin B12 in the urine after absorption and elimination through the kidney. After Vitamin C injection, 1011 cm^{-1} and 952 cm^{-1} , peaks were observed along with regular urine peaks (Figure 11C). And all Vitamin B12 and Vitamin C peaks were observed when injected as a combination (Figure 11D). This indicates the excess Vitamin B12 and Vitamin C eliminates through urine after body absorption, distribution, metabolism, and excretion. This spectral data directly provide the presence of excess vitamins in the urine sample without any alteration or chemical modification of urine during the analysis.

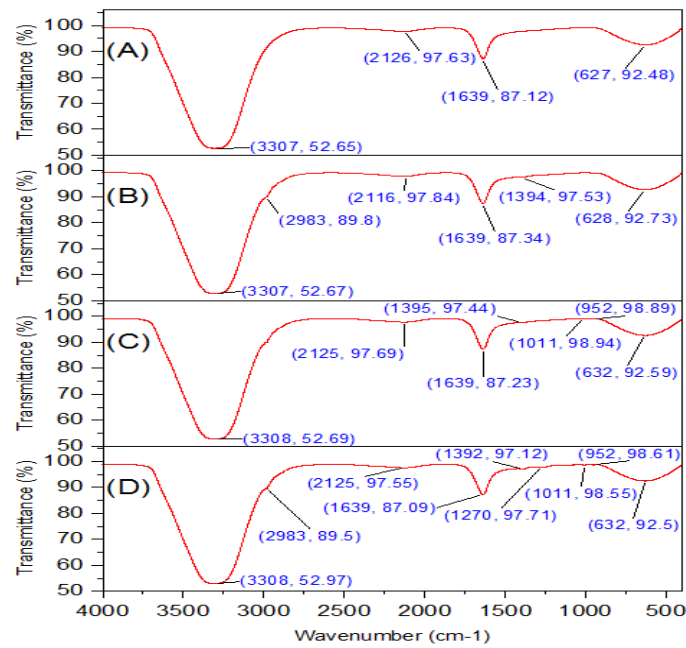


Figure 11. FT-IR spectra of (A) Control rat urine; (B) Vitamin B12 injected rat urine; (C) Vitamin C injected rat urine; (D) Vitamin B12+C injected rat urine.

The FTIR spectra analysis showed the injected vitamins' presence in the tumor-induced rat urine. The new peaks were observed for the Vitamin B12 and Vitamin C injected rat's urine along with normal urea peaks. This indicates the presence of an excess of Vitamin B12 and Vitamin C in the urine after absorption by the body. The FTIR analysis was done with raw urine samples without any chemical modification.

The thermal behavior of the PVDF membrane, Copper nanoparticles, and Graphite paste was analyzed with DSC. PVDF membrane showed an endothermic peak at 65^oC temperature (Figure 12A). This indicates the physical status of fibers in the PVDF membrane. Copper nanoparticles exhibited an endothermic peak at 101^oC (Figure 12B), and graphite paste showed no significant peaks (Figure 12C).

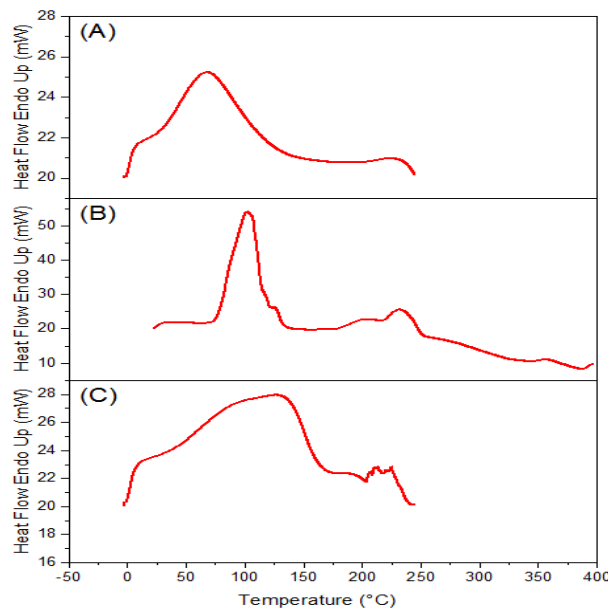


Figure 12. DSC thermographs of (A) PVDF membrane; (B) Copper nanoparticles; (C) Graphite paste.

The DSC data provided the thermal behavior of the PVDF membrane, Copper nanoparticles, and Graphite paste. PVDF membrane exhibited endothermic peaks due to its

fibrous nature, and copper nanoparticles showed endothermic peaks due to their metallic nature. This also indicates these materials can withstand higher temperatures, almost up to 60°C. The graphite paste showed no peaks due to its rich carbon presence.

X-ray diffraction (XRD) patterns of PVDF membrane, Copper nanoparticles, and Graphite paste were recorded. It is shown from Figure 13A that the 2θ peaks corresponding to 18.9° and 24.8° present in the XRD pattern indicate the α -phase in the PVDF membrane. And the presence of a highly intense peak at 19.5° represents the β -phase. Other β -phase peaks at 34.6°, 44.9°, and 55.5° are observed corresponding to the 37.2° and 47.5° α -phase peaks. The presence of both α -phase and β -phase in the XRD pattern indicates the semi-crystalline nature of the PVDF membrane. The peaks of copper nanoparticles were sharp due to their high nanocrystalline property (Figure 13B). The 2θ peaks are observed at 10.5°, 16.2°, and 28.06°. And the lesser impurity peaks showed good crystal distribution in copper nanoparticles. The XRD pattern of graphite paste exhibited high-intensity peaks at 23.6° (Figure 13C). This shows the good crystalline property of graphite.

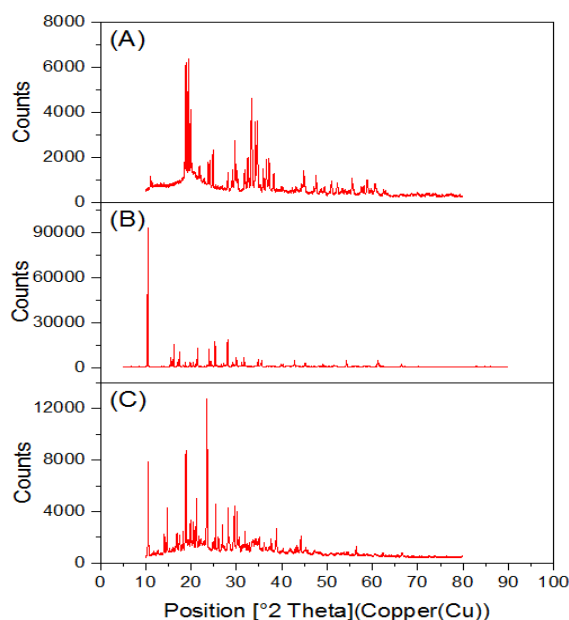


Figure 13. XRD patterns of (A) PVDF membrane; (B) Copper nanoparticles; (C) Graphite paste.

The XRD pattern showed the α -phase and β -phase of the PVDF membrane. This indicates the semi-crystalline property of the PVDF membrane. And the high intensity and sharp peaks of Copper nanoparticles and Graphite paste exhibited their high crystalline property with lesser impurity.

3.3. Mechanical properties of the PVDF cantilever beam.

The deformation occurred in the fabricated PVDF cantilever beam when the sample weights (urine) were applied to the end of the PVDF cantilever beam and which created forces at the free end (Figure 14A). These deformations were analyzed using ANSYS software version 2021 R2 (Figure 14B). The deformation also increases when the weight increases and the cantilever beam starts to bend slightly. In 550 mg (10-11 drops of a processed urine sample) the maximum deflection was observed. This indicates the higher concentrations of excess nutrients and minerals in the tumor-induced rat's urine during excretion. After loading, the PVDF membrane absorbed the sample and moved toward the graphite sensor. The graphite

resistor's ascorbate oxidase (AO) or hydrogen peroxide (H₂O₂) further triggered the deformation due to the oxidation reaction.

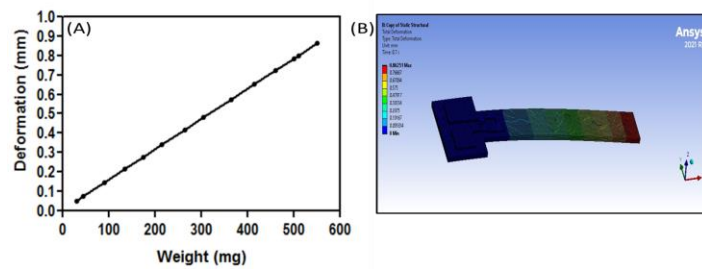


Figure 14. The mechanical properties of the PVDF cantilever beam. (A) The plot of the urine sample weight vs. deformation; (B) PVDF cantilever beam deflections tested in ANSYS 2021 R2.

The ANSYS software version 2021 R2 is used to design the structural layout of the PVDF membrane piezoresistive sensor. The high deformation observed during sample loading (30 mg to 550 mg) was due to the urine concentration and oxidation reaction with the H₂O₂, AO, and luminol. The higher concentrations of excess vitamins excreted through the tumor-induced rat's urine created the maximum deflection and higher oxidation rate. The excess vitamin B12 present in the rat's urine reacts with H₂O₂. The H₂O₂ oxidation on the PVDF membrane produces some reactive oxygen species (ROSs). These reactive species (ROSs), like hydroxyl radical (OH) and superoxide anion (O²⁻), create a reaction with luminol and produce 3-aminophthalate during the excited state. And when it comes back to the ground state, it produces light. The excess vitamin C present in the rat's urine reacts with AO. When vitamin C reaches the graphite sensor, it reacts with AO. The oxidation of luminol occurs in the presence of AO. The reactions were faster when both vitamins were present in the rat's urine. The oxidation of luminol on the reporting side in the presence of H₂O₂ and AO are directly related to the reduction reaction of luminol on the sensing side in the presence of H₂O₂ and AO. The H₂O₂ and AO act as co-reactant in both of these reactions. All these reactions occurred in the graphite sensor for 50-60 seconds when the sample touched the H₂O₂, AO, and luminol. The gas formations during oxidation and reduction reactions can be visible to the naked eye. These oxidation and reduction reactions increased when the weight and quantity of the sample increased. This also supports the resistance change on the PVDF membrane along with the pressure change.

3.4. Electrical properties of graphite resistor.

The prepared graphite resistor exhibited good current-voltage (I-V) characteristics (Figure 15). The graph exhibited a linear curve that indicated ohmic current-voltage (I-V) behavior at 500 Ω resistance under room temperature. The *current I against the potential difference V* showed a straight line as the relation is linear and ohmic. This linear curve indicated ohmic current-voltage (I-V) behavior.

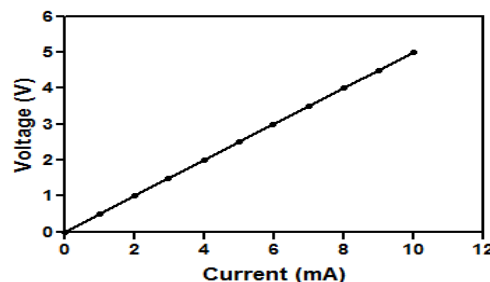


Figure 15. The electrical properties of the graphite resistor.

The assembled POC device abilities were measured under a sterile lab environment at 37°C. The graphite resistor exhibited good current-voltage (I-V) characteristics when tested. The graphite resistor exhibited a linear relationship between current and voltage. When weight (rat's urine sample) is loaded onto the device, the sequential increase in the resistance was observed due to a positive increase in the pressure. When the applied urine sample weight increased from 30 mg to 550 mg, the resistance increased correspondingly due to the contact of the graphite sensor and copper strip through silver ink. The sensitivity changes also occurred due to the increased rate of the contact area between these electrodes. And the sensitivity change gradually slowed down when it reached saturation for the maximum pressure due to the maximum urine sample weight. The characteristics like a wide pressure change, good repeatability, and high sensitivity exhibited excellent performance of flexible pressure sensor-based POC testing.

3.5. Chemical analysis of rat urine.

The oxidation reactions were not visible in the copper strips for ascorbate oxidase (AO), hydrogen peroxide (H₂O₂), and luminol alone (Figure 16). The control urine (tumor-induced rat's urine) also not shown any reaction with the H₂O₂ and AO on the copper strips. But the Vitamin B12 and Vitamin C injected rats' urine exhibited biochemical reactions on the copper strip with H₂O₂ and AO, respectively. The white precipitation was formed during the biochemical reactions with the H₂O₂ and AO. And dense precipitation was visible for the reaction of H₂O₂ and AO with luminol. This was due to the chemiluminescence property of luminol during the oxidation reaction.

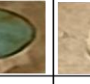



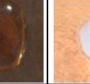

	Urine alone	H ₂ O ₂	AO	LMN	H ₂ O ₂ +AO	H ₂ O ₂ +LMN	AO+LMN	H ₂ O ₂ +AO+LMN
Control urine (Tumour induced rat's urine)	NO 	NO 	NO 	NO 	NO 	NO 	NO 	YES 
Vitamin B12 injected rat's urine	NO 	YES 	NO 	NO 	YES 	YES 	NO 	YES 
Vitamin C injected rat's urine	NO 	YES 	YES 	NO 	YES 	NO 	YES 	YES 
Vitamin B12+ Vitamin C injected rat's urine	NO 	YES 	YES 	NO 	YES 	YES 	YES 	YES 

Figure 16. Chemical analysis of rat's urine with H₂O₂, AO, and luminol (LMN) on the copper nanoparticles coated copper strips.

3.6. Chemiluminescence assay.

The chemiluminescence (CL) intensity is increased when the concentration of the control rat's urine is increased up to 0-50µl and reacted with the H₂O₂, AO, and luminol (Figure

17). But the further increase in urine concentration causes a decrease in the CL intensity. This indicates the increase in urine concentration expedites the chemical reaction and enhances the chemiluminescence up to 50µl. Later the rat's urine became turbid, and chemiluminescence got reduced at high concentrations. The chemiluminescence was also observed for Vitamin B12, and Vitamin C injected tumor rat's urine when reacted with the H₂O₂, AO, and luminol. The CL intensity got increased up to 60µl of urine concentration. Then there was a sudden decrease in the CL intensity due to the turbidity nature of the rat's urine at higher concentrations. The CL intensity of urine with Vitamin B12 was slightly higher than urine with Vitamin C, due to the better oxidation reaction of Vitamin B12 with H₂O₂ and luminol. The same kind of reaction was observed when Vitamin B12 and Vitamin C were injected together. The CL intensity of this sample was much higher for the high urine concentrations compared to urine with Vitamin B12 or Vitamin C. This showed the CL intensity change during the biochemical reactions of excess multivitamins in urine with H₂O₂, AO, and luminol.

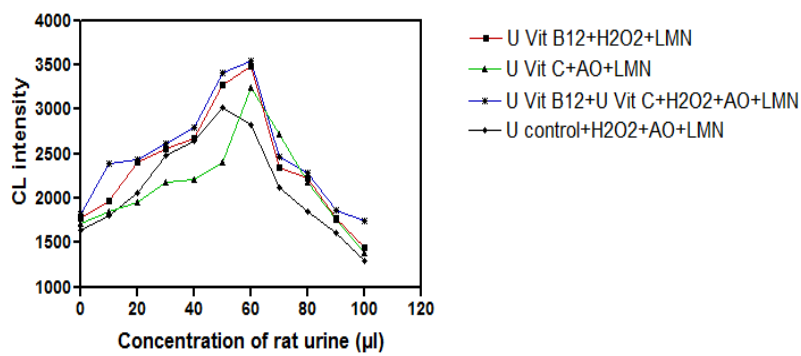


Figure 17. Effect of rat's urine concentration on the CL intensity.

3.7. Performance of hypodermic needle-based POC device.

The resistance change obtained from the digital multimeter (DMM) was observed to increase gradually with the increasing sample weight and oxidation reaction (Figure 18). The resistance change (ΔR) is calculated by the equation:

$$\frac{\Delta R}{R_1} = \frac{(R_1 - R_2)}{R_1} \tag{2}$$

In this formula, R_1 was the initial resistance, and R_2 was the resistance after the stimulation. All tumor-induced rat urine samples exhibited a linear relationship between the resistance change and applied sample weights ranging from 30 mg to 550 mg (1 drop of sample to 10 drops of the tumor-induced rat's urine sample). The resistance change was almost the same for urine with Vitamin B12 and urine with Vitamin C. In contrast, a strong resistance change was observed only for urine with Vitamin B12 and Vitamin C. The Vitamin B12 and Vitamin C injected rat urine samples showed high resistance change while increasing the sample weights. There was a further increase in the resistance value when the oxidation reaction started when the loaded sample reached H₂O₂, AO, and luminol coating. This indicates the resistance change of the graphite sensor in the flexible PVDF membrane cantilever beam during the oxidation reaction while tumor-induced rat urine samples are loaded.

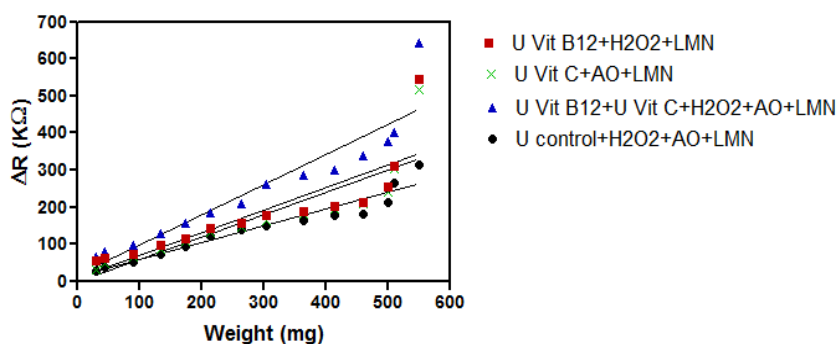


Figure 18. Plot of the relative resistance change vs. the applied urine sample weight.

The performance of the POC device was further clarified by monitoring the oxidation and reduction reaction that occurred when the sample reacted with H₂O₂, AO, and luminol. The pressure change occurred during the decomposition of H₂O₂ and AO with luminol. This pressure change is also monitored with a PVDF membrane-based piezoresistive sensor. The signal readout was detected in the digital multimeter during the breakdown of H₂O₂ and AO with luminol. The different concentrations of rat's urine with vitamin B12 and vitamin C reacted with H₂O₂, AO, and luminol exhibited more feasibility of the POC device. The oxidation and reduction reactions of H₂O₂, AO, and luminol were tested separately on a copper strip placed attached to a glass slide. The H₂O₂, AO, luminol, and urine without vitamins (control) not show any reaction on the copper strip. But the Vitamin B12 and Vitamin C injected rats' urine exhibited biochemical reactions with H₂O₂, AO, and luminol on the copper strip by producing gases followed by white precipitation. This confirms the chemiluminescence property of luminol during the oxidation and reduction reaction on the PVDF membrane. Chemiluminescence (CL) intensity was also measured under a microplate reader on a 96-well optic plate. The CL intensity increased when the concentration of the tumor-induced rat's urine sample increased from 0-50μl for the control rat's urine, and 0-60μl for Vitamin B12 and Vitamin C injected tumor rat's urine. But the CL intensity got decreased beyond that concentration due to H₂O₂ and AO breakdown with luminol while reacting with more turbid urine. The reactive species in the H₂O₂ and AO controlled the chemiluminescence at higher urine concentrations. The CL intensity of urine with Vitamin B12 was slightly higher than urine with Vitamin C because H₂O₂ easily decomposes under ambient conditions than AO. In contrast, the CL intensity largely increased when adding Vitamin B12 and Vitamin C injected rats' urine samples into the wells. This indicates the sensitive monitoring of chemiluminescence property during the decomposition of H₂O₂ and AO with luminol while adding the tumor-induced rat's urine.

The sensitivity and ability were further evaluated by assaying different concentrations of tumor-induced rat urine samples under optimal conditions. The precision and reproducibility of the POC device were analyzed by loading different concentrations of tumor-induced rat urine samples. The applied weight of all urine samples exhibited a linear relationship with the resistance change. This shows this POC device's user-friendly and quick application during pre and post-cancer treatments. The POC device was also conducted with PVDF membrane sensors stored for 5-6 months. Almost the same results were observed for long-time stored PVDF membrane sensors as well. This indicates long-term stability and high specificity of hypodermic needle-based POC devices. Thus this POC device may also be used for cancer patients' urine samples to quickly detect Vitamin B12 and Vitamin C presence pre and post-chemotherapy.

4. Conclusions

The current pre and post-cancer treatments mainly focus on the patients' pain management, cure, and survival through radiation, chemotherapy, surgery, hormonal treatments, or immunotherapy. The vitamin status of these patients during these treatments is not a major consideration unless it leads to malnutrition or prolonged side effects of chemotherapeutic drugs. The correct vitamin diagnosis at frequent intervals is very important for these patients in day-to-day life without any frequent visits to labs or hospitals. The advantages of our hypodermic needle-based POC device for vitamin B12 and Vitamin C detection are reliability, high sensitivity, and high specificity. This POC device is inexpensive (~25 Rs. per device), easy to fabricate, lightweight, disposable, and recyclable. This device was made to analyze the biochemical reaction of excess vitamins present in the urine with the help of a flexible PVDF membrane-based piezoresistive sensor. The signals were detected with the help of a digital multimeter. The resistance change followed by pressure change by tumor-induced rat's urine sample due to the decomposition of H₂O₂ and AO with luminol was also easily monitored with this POC device. With this affordable and portable device, cancer patients' urine samples may easily be analyzed at any time or in any remote area.

Funding

This research received no external funding.

Acknowledgments

The authors thank the CSIR-Indian Institute of Chemical Technology (CSIR-IICT), Hyderabad, India, and the CSIR-Centre for Cellular and Molecular Biology (CCMB), Hyderabad, India, for conducting the characterization studies.

Conflicts of Interest

The authors declare no conflict of interest.

References

1. Bodai, B. I.; Tuso, P. Breast Cancer Survivorship: A Comprehensive Review of Long-Term Medical Issues and Lifestyle Recommendations. *Perm J.* **2015**, *19*, 48–79, <https://doi.org/10.7812/TPP/14-241>.
2. Conigliaro, T.; Boyce, L. M.; Lopez, C. A.; Tonorezos, E. S. Food Intake During Cancer Therapy: A Systematic Review. *American journal of clinical oncology* **2020**, *43*, 813–819, <https://doi.org/10.1097/COC.0000000000000749>.
3. Kim, D. H. Nutritional Issues in Patients with Cancer. *Intest Res* **2019**, *17*, 455–462, <https://doi.org/10.5217/ir.2019.00076>.
4. Chen, L.; Qi, Y.; Kong, X.; Su, Z.; Wang, Z.; Wang, X.; Du, Y.; Fang, Y.; Li, X.; Wang, J. Nutritional Risk Index Predicts Survival in Patients With Breast Cancer Treated With Neoadjuvant Chemotherapy. *Front Nutr* **2021**, *8*, 786742, <https://doi.org/10.3389/fnut.2021.786742>.
5. Cable, R. G.; Steele, W. R.; Melmed, R. S.; Johnson, B.; Mast, A. E.; Carey, P. M.; Kiss, J. E.; Kleinman, S. H.; Wright, D. J.; NHLBI Retrovirus Epidemiology Donor Study-II (REDS-II). The Difference between Fingerstick and Venous Hemoglobin and Hematocrit Varies by Sex and Iron Stores. *Transfusion (Paris)* **2012**, *52*, 1031–1040, <https://doi.org/10.1111/j.1537-2995.2011.03389.x>.
6. Boroumand, M.; Olianias, A.; Cabras, T.; Manconi, B.; Fanni, D.; Faa, G.; Desiderio, C.; Messina, I.; Castagnola, M. Saliva, a bodily fluid with recognized and potential diagnostic applications. *Journal of separation science* **2021**, *44*, 3677–3690, <https://doi.org/10.1002/jssc.202100384>.

7. Lee, W.; Kim, Y.; Chang, S.; Lee, A.-J.; Jeon, C.-H. The Influence of Vitamin C on the Urine Dipstick Tests in the Clinical Specimens: A Multicenter Study. *J Clin Lab Anal* **2017**, *31*, <https://doi.org/10.1002/jcla.22080>.
8. Ravasco, P. Nutrition in Cancer Patients. *J Clin Med* **2019**, *8*, 1211, <https://doi.org/10.3390/jcm8081211>.
9. Cool, L.; Callewaert, N.; Pottel, H.; Mols, R.; Lefebvre, T.; Tack, L.; Lycke, M.; Missiaen, J.; Debruyne, P.; Vandijck, D.; et al. Quality of Blood Samples Collected at Home Does Not Affect Clinical Decision Making for the Administration of Systemic Cancer Treatment. *Scand J Clin Lab Invest* **2020**, *80*, 215–221, <https://doi.org/10.1080/0036513.2020.1716267>.
10. Cree, I. A.; Deans, Z.; Ligtenberg, M. J. L.; Normanno, N.; Edsjö, A.; Rouleau, E.; Solé, F.; Thunnissen, E.; Timens, W.; Schuurin, E.; et al. Guidance for Laboratories Performing Molecular Pathology for Cancer Patients. *J Clin Pathol* **2014**, *67*, 923–931, <https://doi.org/10.1136/jclinpath-2014-202404>.
11. Koonmee, S.; Sangkhamanon, S.; Intarawichian, P.; Aphivatanasiri, C.; Kunprom, W.; Sa-Ngiamwibool, P.; Balthaisong, S.; Phuyao, C.; Prajumwongs, P.; Alaghehbandan, R.; Thanee, M. The Impact of Pre-analytical Quality Initiatives on Cholangiocarcinoma Diagnostics in Thailand. *Frontiers in public health* **2022**, *10*, 792847, <https://doi.org/10.3389/fpubh.2022.792847>.
12. Bhalla, N.; Jolly, P.; Formisano, N.; Estrela, P. Introduction to Biosensors. *Essays Biochem* **2016**, *60*, 1–8, <https://doi.org/10.1042/EBC20150001>.
13. Su, Y.; Ma, K.; Yuan, F.; Tang, J.; Liu, M.; Zhang, X. High-Performance Flexible Piezoresistive Sensor Based on Ti3C2Tx MXene with a Honeycomb-like Structure for Human Activity Monitoring. *Micromachines* **2022**, *13*, 821, <https://doi.org/10.3390/mi13060821>.
14. Huang, L.; Tian, S.; Zhao, W.; Liu, K.; Guo, J. Electrochemical Vitamin Sensors: A Critical Review. *Talanta* **2021**, *222*, 121645, <https://doi.org/10.1016/j.talanta.2020.121645>.
15. Shadjou, N.; Hasanzadeh, M.; Omari, A. Electrochemical Quantification of Some Water Soluble Vitamins in Commercial Multi-Vitamin Using Poly-Amino Acid Caped by Graphene Quantum Dots Nanocomposite as Dual Signal Amplification Elements. *Anal Biochem* **2017**, *539*, 70–80, <https://doi.org/10.1016/j.ab.2017.10.011>.
16. Punetha, D.; Kar, M.; Pandey, S. K. A New Type Low-Cost, Flexible and Wearable Tertiary Nanocomposite Sensor for Room Temperature Hydrogen Gas Sensing. *Sci Rep* **2020**, *10*, 2151, <https://doi.org/10.1038/s41598-020-58965-w>.
17. Liu, Y.; Wang, H.; Zhao, W.; Qin, H.; Fang, X. Thermal-Performance Instability in Piezoresistive Sensors: Inducement and Improvement. *Sensors* **2016**, *16*, 1984, <https://doi.org/10.3390/s16121984>.
18. Iqra, M.; Anwar, F.; Jan, R.; Mohammad, M. A. A Flexible Piezoresistive Strain Sensor Based on Laser Scribed Graphene Oxide on Polydimethylsiloxane. *Sci Rep* **2022**, *12*, 4882, <https://doi.org/10.1038/s41598-022-08801-0>.
19. Wang, X.; Li, H.; Wang, T.; Niu, X.; Wang, Y.; Xu, S.; Jiang, Y.; Chen, L.; Liu, H. Flexible and High-Performance Piezoresistive Strain Sensors Based on Multi-Walled Carbon Nanotubes@polyurethane Foam. *RSC Adv* **2022**, *12*, 14190–14196, <https://doi.org/10.1039/d2ra01291j>.
20. Li, T.; Shang, H.; Wang, W. Simulation and Nonlinearity Optimization of a High-Pressure Sensor. *Sensors* **2020**, *20*, 4419, <https://doi.org/10.3390/s20164419>.
21. Zhang, Y.; Li, L. Modelling and Design of MEMS Piezoresistive Out-of-Plane Shear and Normal Stress Sensors. *Sensors* **2018**, *18*, 3737, <https://doi.org/10.3390/s18113737>.
22. Nayak, S.; Blumenfeld, N. R.; Laksanasopin, T.; Sia, S. K. Point-of-Care Diagnostics: Recent Developments in a Connected Age. *Anal Chem* **2017**, *89*, 102–123, <https://doi.org/10.1021/acs.analchem.6b04630>.
23. Bharadwaj, M.; Bengtson, M.; Golverdingen, M.; Waling, L.; Dekker, C. Diagnosing point-of-care diagnostics for neglected tropical diseases. *PLoS neglected tropical diseases* **2021**, *15*, e0009405, <https://doi.org/10.1371/journal.pntd.0009405>.
24. Lei, R.; Huo, R.; Mohan, C. Current and emerging trends in point-of-care urinalysis tests. *Expert review of molecular diagnostics* **2020**, *20*, 69–84, <https://doi.org/10.1080/14737159.2020.1699063>.
25. Yang, S.-M.; Lv, S.; Zhang, W.; Cui, Y. Microfluidic Point-of-Care (POC) Devices in Early Diagnosis: A Review of Opportunities and Challenges. *Sensors* **2022**, *22*, 1620, <https://doi.org/10.3390/s22041620>.
26. Wang, C.; Liu, M.; Wang, Z.; Li, S.; Deng, Y.; He, N. Point-of-Care Diagnostics for Infectious Diseases: From Methods to Devices. *Nano Today* **2021**, *37*, 101092, <https://doi.org/10.1016/j.nantod.2021.101092>.
27. Mehrotra, P. Biosensors and Their Applications - A Review. *J Oral Biol Craniofac Res* *6*, 153–159, <https://doi.org/10.1016/j.jobcr.2015.12.002>.
28. Meng, Y.; Li, H.; Wu, K.; Zhang, S.; Li, L. High-Performance Pressure Sensor for Monitoring Mechanical Vibration and Air Pressure. *Polymers* **2018**, *10*, 587, <https://doi.org/10.3390/polym10060587>.

29. Liu, D.; Tian, T.; Chen, X.; Lei, Z.; Song, Y.; Shi, Y.; Ji, T.; Zhu, Z.; Yang, L.; Yang, C. Gas-Generating Reactions for Point-of-Care Testing. *Analyst* **2018**, *143*, 1294–1304, <https://doi.org/10.1039/C8AN00011E>.
30. Fernández, L.; Alvarez-Paguay, J.; González, G.; Uribe, R.; Bolaños-Mendez, D.; Piñeiros, J. L.; Celi, L.; Espinoza-Montero, P. J. Electrochemical Sensor for Hydrogen Peroxide Based on Prussian Blue Electrochemically Deposited at the TiO₂-ZrO₂-Doped Carbon Nanotube Glassy Carbon-Modified Electrode. *Front Chem* **2022**, *10*, 884050, <https://doi.org/10.3389/fchem.2022.884050>.
31. Zambrano, G.; Natri, F.; Pavone, V.; Lombardi, A.; Chino, M. Use of an Artificial Miniaturized Enzyme in Hydrogen Peroxide Detection by Chemiluminescence. *Sensors* **2020**, *20*, 3793, <https://doi.org/10.3390/s20133793>.
32. Li, Q.; Zhang, Y.; Li, P.; Xue, H.; Jia, N. A Nanocomposite Prepared from Hemin and Reduced Graphene Oxide Foam for Voltammetric Sensing of Hydrogen Peroxide. *Mikrochim Acta* **2019**, *187*, 45, <https://doi.org/10.1007/s00604-019-3829-3>.
33. Fu, Q.; Wu, Z.; Li, J.; Wu, Z.; Zhong, H.; Yang, Q.; Liu, Q.; Liu, Z.; Sheng, L.; Xu, M.; et al. Quantitative Assessment of Disease Markers Using the Naked Eye: Point-of-Care Testing with Gas Generation-Based Biosensor Immunochromatographic Strips. *J Nanobiotechnology* **2019**, *17*, 67, <https://doi.org/10.1186/s12951-019-0493-z>.
34. Lu, C.; Han, J.; Sun, X.; Yang, G. Electrochemical Detection and Point-of-Care Testing for Circulating Tumor Cells: Current Techniques and Future Potentials. *Sensors* **2020**, *20*, 6073, <https://doi.org/10.3390/s20216073>.
35. Zheng, W.; Xu, H.; Wang, M.; Duan, Q.; Yuan, Y.; Wang, W.; Gao, L. On-Skin Flexible Pressure Sensor with High Sensitivity for Portable Pulse Monitoring. *Micromachines* **2022**, *13*, 1390, <https://doi.org/10.3390/mi13091390>.
36. Kalimuldina, G.; Turdakyn, N.; Abay, I.; Medeubayev, A.; Nurpeissova, A.; Adair, D.; Bakenov, Z. A Review of Piezoelectric PVDF Film by Electrospinning and Its Applications. *Sensors* **2020**, *20*, 5214, <https://doi.org/10.3390/s20185214>.
37. Singh, A. T.; Lantigua, D.; Meka, A.; Taing, S.; Pandher, M.; Camci-Unal, G. Paper-Based Sensors: Emerging Themes and Applications. *Sensors* **2018**, *18*, 2838, <https://doi.org/10.3390/s18092838>.
38. Al-Saygh, A.; Ponnamma, D.; AlMaadeed, M. A.; Vijayan P, P.; Karim, A.; Hassan, M. K. Flexible Pressure Sensor Based on PVDF Nanocomposites Containing Reduced Graphene Oxide-Titania Hybrid Nanolayers. *Polymers* **2017**, *9*, 33, <https://doi.org/10.3390/polym9020033>.
39. Martin, K.; Wenlock, R.; Roper, T.; Butler, C.; Vera, J. H. Facilitators and barriers to point-of-care testing for sexually transmitted infections in low- and middle-income countries: a scoping review. *BMC infectious diseases* **2022**, *22*, 561, <https://doi.org/10.1186/s12879-022-07534-9>.
40. Chen, H.; Liu, K.; Li, Z.; Wang, P. Point of Care Testing for Infectious Diseases. *Clin Chim Acta* **2019**, *493*, 138–147, <https://doi.org/10.1016/j.cca.2019.03.008>.
41. Konwar, A. N.; Borse, V. Current Status of Point-of-Care Diagnostic Devices in the Indian Healthcare System with an Update on COVID-19 Pandemic. *Sensors international* **2020**, *1*, 100015, <https://doi.org/10.1016/j.sintl.2020.100015>.
42. Hess, K. L.; Fisher, D. G.; Reynolds, G. L. Sensitivity and Specificity of Point-of-Care Rapid Combination Syphilis-HIV-HCV Tests. *PLoS One* **2014**, *9*, e112190, <https://doi.org/10.1371/journal.pone.0112190>.
43. Wang, S.; Lifson, M. A.; Inci, F.; Liang, L.-G.; Sheng, Y.-F.; Demirci, U. Advances in Addressing Technical Challenges of Point-of-Care Diagnostics in Resource-Limited Settings. *Expert Rev Mol Diagn* **2016**, *16*, 449–459, <https://doi.org/10.1586/14737159.2016.1142877>.
44. Malhotra, B. D.; Ali, Md. A. Nanomaterials in Biosensors. In *Nanomaterials for Biosensors* **2018**, 1–74, <https://doi.org/10.1016/B978-0-323-44923-6.00001-7>.
45. Crole, D. A.; Underhill, R.; Edwards, J. K.; Shaw, G.; Freakley, S. J.; Hutchings, G. J.; Lewis, R. J. The Direct Synthesis of Hydrogen Peroxide from H₂ and O₂ Using Pd-Ni/TiO₂ Catalysts. *Philos Trans A Math Phys Eng Sci* **2020**, *378*, 20200062, <https://doi.org/10.1098/rsta.2020.0062>.
46. Antunes, F.; Brito, P. M. Quantitative Biology of Hydrogen Peroxide Signaling. *Redox Biol* **2017**, *13*, 1–7, <https://doi.org/10.1016/j.redox.2017.04.039>.
47. Meng, Q.; Lu, Y.; Wang, J.; Chen, D.; Chen, J. A Piezoresistive Pressure Sensor with Optimized Positions and Thickness of Piezoresistors. *Micromachines*, **2021**, *12*, 1095, <https://doi.org/10.3390/mi12091095>.
48. Vashist, S. K. Point-of-Care Diagnostics: Recent Advances and Trends. *Biosensors* **2017**, *7*, 62, <https://doi.org/10.3390/bios7040062>.

49. Iliescu, F. S.; Ionescu, A. M.; Gogianu, L.; Simion, M.; Dediu, V.; Chifiriuc, M. C.; Pircalabioru, G. G.; Iliescu, C. Point-of-Care Testing-The Key in the Battle against SARS-CoV-2 Pandemic. *Micromachines* **2021**, *12*, 1464, <https://doi.org/10.3390/mi12121464>.
50. Sachdeva, S.; Davis, R. W.; Saha, A. K. Microfluidic Point-of-Care Testing: Commercial Landscape and Future Directions. *Front Bioeng Biotechnol* **2020**, *8*, 602659, <https://doi.org/10.3389/fbioe.2020.602659>.
51. Guo, S.; Duan, X.; Xie, M.; Aw, K. C.; Xue, Q. Composites, Fabrication and Application of Polyvinylidene Fluoride for Flexible Electromechanical Devices: A Review. *Micromachines* **2020**, *11*, 1076, <https://doi.org/10.3390/mi11121076>.
52. Ruan, L.; Yao, X.; Chang, Y.; Zhou, L.; Qin, G.; Zhang, X. Properties and Applications of the β Phase Poly(Vinylidene Fluoride). *Polymers* **2018**, *10*, 228, <https://doi.org/10.3390/polym10030228>.
53. Gontarek-Castro, E.; di Luca, G.; Lieder, M.; Gugliuzza, A. Graphene-Coated PVDF Membranes: Effects of Multi-Scale Rough Structure on Membrane Distillation Performance. *Membranes* **2022**, *12*, 511, <https://doi.org/10.3390/membranes12050511>.
54. Liu, M.; Liu, Y.; Zhou, L. Novel Flexible PVDF-TrFE and PVDF-TrFE/ZnO Pressure Sensor: Fabrication, Characterization and Investigation. *Micromachines* **2021**, *12*, 602, <https://doi.org/10.3390/mi12060602>.